Research Article

Numerical Simulation of Granular Flow in Concrete Batching Plant via Discrete Element Method

Jaber Salamat[1*], Bülent Genç[2*]

[1] Elkon Concrete Batching Plants, R&D Center, Tekirdağ, Türkiye, Orcid ID: 0000-0003-0491-745X, E-mail: jaber@elkonarge.com
[2] Elkon Concrete Batching Plants, R&D Center, Tekirdağ, Türkiye, Orcid ID: 0000-0001-8093-808X, E-mail: bulent.genc@elkon.net
[*] Correspondence: jaber@elkonarge.com

(First received January 27, 2023 and in final form May 11, 2023)

Reference: Comparison of Water Discharge Performance of Motorcycle Tires with Different Tread Patterns by Applying CFD (Computational Fluid Dynamics) Technique. The European Journal of Research and Development,3(2), 11–28.

Abstract

A new giant concrete batching plant with the production capacity of $\mathbf{270\ m^3/hr}$ *was designed, analyzed and fabricated. In this concrete batching plant, the granular materials used for high-quality products must be uniformly mixed to attain a homogenous mixture. For this, the discrete element method (DEM) was utilized to simulate the filling, mixing, and discharging processes. The Hertz-Mindlin, elastic-plastic spring-dashpot and Simplified Johnson-Kendall-Roberts (SJKR) models were used for the interaction rules among granular particles. In the light of the aforementioned models, the first simulation with different particle sizes and the second simulation with monosized particles were realized. In the first simulation, the segregation by percolation and momentum segregation were perceived during the bunker filling stage, as well as the seeded granulation, which occurred in the mixer when the radii of particles were not monosized. Furthermore, in the second simulation, convective, diffusive and shear mixing mechanisms were observed and consequently the quantification of the mixing index was calculated using the lacey and miles statistical methods. At last, the active regions formed in the mixer were investigated by taking the velocity of the particles as reference during the mixing stages as well as the mixture throughput from the transfer chute.*

Keywords: *Discrete Element Method, Granular Materials, Twin Shaft Mixer, Wet Granulation*

1. Introduction

Particle mixing is a fundamental process in many industrial applications such as food, cosmetics, metallurgy, coal, pharmaceutical, plastics, cement and concrete manufacturing. Annually, over a trillion kilograms of granular and powdered products are processed, much of which must be uniformly blended to meet specific quality and

goals [1]. The goal has been reached by designing a variety of mixers, including batch and continuous, where design, control and optimization of these systems are challenging tasks to meet an efficient process design [2]. In the light of DEM, besides simulation and visualization of the material flow, it is also possible to analyze forces and moments on different components of the system. Therefore, the wear of the system components will be predictable to optimize the system performance for an increased lifetime [3]. There has been considerable research on granular [4,5] and powder [6,7] mixing to simulate the characteristics of different materials in the literature. Several mechanisms including convection, shear, diffusion and percolation have been introduced for mixing and de-mixing of granular materials [8-11]. The goal of these mechanisms is the realization of homogeneous material using the minimum amount of energy and time. On the other hand, simulation challenges will appear due to the diversity of granules in terms of size, shape, density, moisture, cohesive and non-cohesive particles [12,13]. Therefore, granular mixing is more complex phenomenon in comparison to fluid mixing, which leads to segregation due to those aforementioned granule properties. Also, the size and density differences are the most and less important properties, respectively, in comparison to other granules characteristics.

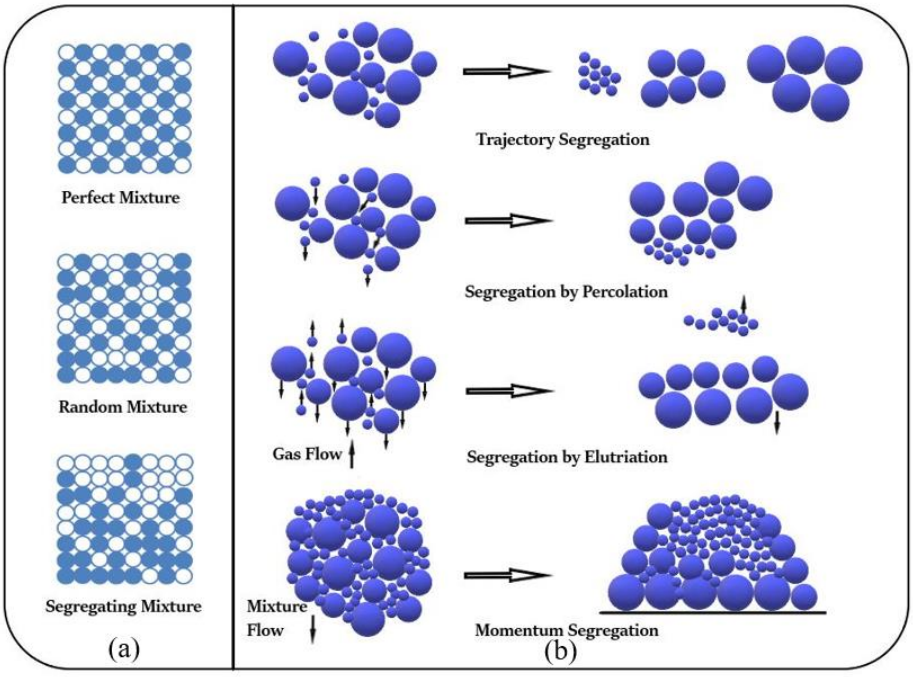

Figure 1. Different types of mixtures (a) and segregation mechanisms (b) [14,18]

As shown in Fig. 1(a), three mixture types have been reported in the literature, namely, perfect mixture, random mixture and segregating mixture [14]. The segregation of particles is an opposing mechanism to the mixing, which occurs during mixing and when

the mixer is switched off. Thus, the segregation mechanisms should be understood very well to avoid this phenomenon. On the other hand, cohesive particles are less prone to segregate because the forces between particles hinder the segregation to a certain degree. But, non-cohesive particles having different characteristics are vulnerable to segregation because of collisional contacts arisen from their high kinetic energies. Fig. 1(b) shows four segregation mechanisms including trajectory, percolation, elutriation, and momentum segregation which have been investigated in previous works [15-18]. These segregation mechanisms will be discussed in detail over the full model of 6 m^3 twin shaft mixer (TSM) which is fully equipped with a mega bunker and controllable double side transfer chute.

In this study, a giant concrete batching plant with the full production capacity of 270 m^3/hr was designed, analyzed and fabricated. This machine consists of three main sections: the mega bunker, the 6 m^3 TSM and the transfer chute. The mega bunker is designed so that to have a high capacity with two areas that store aggregates and cement separately but discharge them together with two hydraulically controllable pouring gates into the mixer. Also, the mixer is a 6 m^3 twin shaft equipped with specially designed robust blades and arms to mix the granules with high homogeneity. In addition, the transfer chute is designed in order to guide the pouring fresh concrete to two sides with a specially designed automatic apron. For the evaluation of 6 m^3 TSM, the homogeneity rates are calculated by the lacey and miles mixing index methods, and the results fulfilled the project goals very well. The DEM can be used to study the physical and mechanical characteristics of different granular materials in the systems using various commercial and open source programs. Numerical simulations for discharging, mixing, and pouring performance of the bunker and mixer simultaneously are realized in real industrial size via LIGGGHTS 3.0, Open Source DEM Particle Simulation Software. LIGGGHTS stands for "LAMMPS Improved for General Granular and Granular Heat Transfer Simulations" and is based on LAMMPS ("Large Atomic and Molecular Massively Parallel Simulator"), an open source molecular dynamics code by Sandia National Laboratories for massively parallel computing on distributed memory machines [19,20]. Recently, commercial software: EDEM, ROCKY, NEWTON and PASSAGE/DEM as well as open source programs: LIGGGHTS, YADE, MERCURY DPM and LMGC90 have been developed by many research groups. Commercial software are usually costly and often limit a researcher's ability to improve the existing codes. Therefore, we developed and adopted the LIGGGHTS UDF codes to simulate our needs.

2. Materials and Methods

Several discrete modeling techniques have been developed such as the Monte Carlo method, cellular automata, smooth particle hydrodynamics (SPH), and DEM [21-23]. The discrete element method is a Lagrangian method, which can provide dynamic information related to particle motions trajectories, velocities of particles, and forces

acting on individual particles [24]. Fig. 2 shows the interaction forces between particles represented by the springs and a dashpot, simulating the elastic and plastic nature of particles in the normal direction, respectively [25-27]. On the other hand, the interaction forces between particles in the tangential direction are represented by the sliders, springs, and a dashpot. The following two equations demonstrate the translational and angular movement of each granular particle in a system exposed to particle/particle, particle to a wall, blade interactions, cohesive forces and gravity as well.

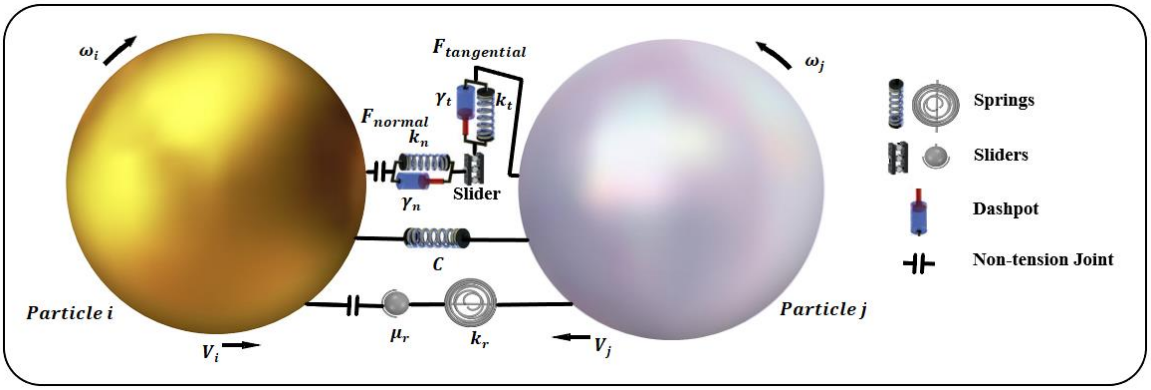

Figure 2. Model of force/torque interactions between two particles [26]

$$m_i \frac{dV_i}{dt} = \sum_{j=1}^{K_i}(F_{c,ij}^n + F_{d,ij}^n + F_{c,ij}^t + F_{d,ij}^t) + \sum_{j=1}^{N_i}(F_{v,ij}) + m_i g \quad (1)$$

$$I_i \frac{d\omega_i}{dt} = \sum_{j=1}^{K_i}(T_{ij}^t + T_{ij}^r) \quad (2)$$

Here, m_i, I_i, K_i, V_i and ω_i are mass, moment of inertia, number of particles in contact with particle i, translational and angular velocity of particle, respectively. The forces are inter-particle, cohesive and gravitation. Here, $F_{c,ij}^n$ and $F_{d,ij}^n$ are the contact and damping forces in the normal direction along with $F_{c,ij}^t$ and $F_{d,ij}^t$ which stand for the contact and damping forces in the tangential direction, respectively. Also, $F_{v,ij}$ is the cohesive force between particles i and j as well as N_i which is the number of particles in the immediate neighborhood of particle i. The torques resulting from the tangential force and rolling friction are represented by T_{ij}^t and T_{ij}^r, respectively. All of the forces and torques are calculated based on the interaction and the physical properties of particles. For the calculation of these forces, several contact models have been developed such as elastic and inelastic as well as non-contact techniques.

2.1. Contact Models

The DEM considering various contact theories have been gradually developed and improved to simulate more complex behaviors of granular materials. The elastic contact

theories are differentiated into two main categories as linear (Linear Spring Model) and non-linear (Hertz-Mindlin Model, Hertz-Mindlin+Johnson-Kendall-Roberts (JKR) Model, Derjaguin-Muller-Toporov (DMT) Model) [28-31]. On the other hand, inelastic contact theories are linear spring-dashpot model, hysteretic model, and Thornton model [32-34]. Also, non-contact particle interactions are divided into three parts including liquid bridge force, Van der Waals force and electrostatic force models. The explanations of aforementioned studies are beyond the scope of this paper but in the forthcoming sections the hertz, JKR and SJKR models are discussed in more detail with mathematical formulas which are implemented by C++ for the successful simulation in this study.

2.1.1. Hertz-mindlin Contact Model

A pioneering paper published by Heinrich Hertz on the normal contact of elastic spheres and his theoretical study on the equations of interaction is referred to as Hertz theory [35]. This theory determines the forces due to the collisional contact between two particles. The impact force resulting from a collision of two elastic and rigid particles is calculated from very small normal (δ_n) and tangential (δ_t) overlaps by Hertz-Mindlin's contact law. These contact forces can be determined at each time step of simulation by the following equation:

$$F = (k_n \delta_{n,ij} - \gamma_n \mathrm{v}_{n,ij})) + (k_t \delta_{t,ij} - \gamma_t \mathrm{v}_{t,ij}) \quad (3)$$

This granular model uses the above equation for the frictional force between two granular particles when the distance l_{ij} between two particles of radii R_i and R_j is less than their constant distance $d = R_i + R_j$. Also, there is no force between the particles when $l_{ij} > d$. In Eq. (3), the first and the second terms stand for normal and tangential forces, respectively. In the first term, k_n, $\delta_{n,ij}$, γ_n and $\mathrm{v}_{n,ij}$ are the elastic constant for normal contact, normal overlap, viscoelastic damping constant for normal contact and normal component of the relative velocity of the two particles, sequentially. In the second term, k_t is elastic constant for tangential contact, $\delta_{t,ij}$ is tangential overlap, γ_t is viscoelastic damping constant for tangential contact and $\mathrm{v}_{t,ij}$ is tangential relative velocity, respectively.

Static friction is obtained by keeping track of the elastic shear displacement during the lifetime of the contact. The magnitude of the tangential overlap is truncated as necessary to satisfy a local Coulomb yield criterion: $(F^t_{c,ij} + F^t_{d,ij}) \leq \mu(F^n_{c,ij} + F^n_{d,ij})$, where μ is the grain-grain friction coefficient. Therefore, the constant surfaces are treated as sticking when $(F^t_{c,ij} + F^t_{d,ij}) < \mu(F^n_{c,ij} + F^n_{d,ij})$, and as slipping when the Coulomb yield criterion is satisfied [36]. According to the Hertz-Mindlin model, the k_n, γ_n, k_t, and γ_t coefficients are calculated by the following equations:

$$k_n = \frac{4}{3}E^*\sqrt{R^*\delta_n} \quad (4)$$

$$\gamma_n = -2\sqrt{\frac{5}{6}}\beta\sqrt{S_n m^*} \geq 0 \quad (5)$$

$$k_t = 8G^*\sqrt{R^*\delta_n} \quad (6)$$

$$\gamma_t = -2\sqrt{\frac{5}{6}}\beta\sqrt{S_t m^*} \geq 0 \quad (7)$$

The coefficients S_n, S_t, β, E^*, G^*, R^* and m^* can be defined using the following equations:

$$S_n = 2E^*\sqrt{R^*\delta_n} \quad (8)$$

$$S_t = 8G^*\sqrt{R^*\delta_n} \quad (9)$$

$$\beta = \frac{\ln(e)}{\sqrt{\ln^2(e)+\pi^2}} \quad (10)$$

$$\frac{1}{E^*} = \frac{(1-v_i^2)}{E_i} + \frac{(1-v_j^2)}{E_j} \quad (11)$$

$$\frac{1}{G^*} = \frac{2(2+v_i)(1-v_i)}{E_i} + \frac{2(2+v_j)(1-v_j)}{E_j} \quad (12)$$

$$\frac{1}{R^*} = \frac{1}{R_i} + \frac{1}{R_j} \quad (13)$$

$$\frac{1}{m^*} = \frac{1}{m_i} + \frac{1}{m_j} \quad (14)$$

where E, G, v, e, m and R are Young's modulus, shear modulus, Poisson's ratio, coefficient of restitution, mass and radius of particle, respectively.

Open-source LIGGGHTS code has been used in this study through the realization of Hertz-Mindlin law and elastic-plastic spring-dashpot model [19] in feeding the mega bunker. Also, mechanical and physical properties of the granular materials have been utilized in the simulation. To study the mixing performance of 6 m^3 TSM, SJKR contact model has been applied in the simulation and the seeded granulation process has been perceived. SJKR is a modified simplified Johnson-Kendall-Roberts cohesion model, which is used to simulate the cohesion of particles.

2.1.2. JKR Contact Model

Hertz-Mindlin's contact law does not take into account the attractive forces between the granular particles. Johnson et al. [30] derived the JKR theoretical model using the principle of minimum energy which considers the effect of surface energy. In JKR theory, normal force and particle overlap are calculated by the following equations [37]:

$$F_n = \frac{4E^* a^3}{3R^*} - (8\pi\xi E^* a^3)^{1/2} \tag{15}$$

$$\delta_n = \frac{a^2}{R^*} - (\frac{2\pi\xi a}{E^*})^{1/2} \tag{16}$$

where ξ, a, E^* and R^* are surface energy, particle contact spot radius, effective Young's modulus and effective radius of contacting bodies, respectively. If there is no adhesion between particles, the second term in Eqs. (15) and (16) disappear and the JKR contact model reduces to Hertz-Mindlin contact model. We use SJKR model for highly adhesive materials. To maintain a large contact area, an additional normal force is added to the Hertzian contact law, given by

$$F_{Coh} = CA \tag{17}$$

where C is the cohesion energy density and A is the particle contact area, given as:

$$A = \frac{\pi}{4}\frac{(l_{ij}-R_i-R_j)(l_{ij}+R_i-R_j)(l_{ij}-R_i+R_j)(l_{ij}+R_i+R_j)}{l_{ij}{}^* l_{ij}} \tag{18}$$

Here, R_i and R_j are the radii of spherical particles i and j, respectively, and l_{ij} stands for the distance between particle centers.

2.2. Physical Model and Simulation

As shown in Fig. 3(a) and (b), the giant batching plant assembly operation view and top view from inside the 6 m^3 TSM are illustrated. The plant consists of a mega bunker, a 6 m^3 TSM and a transfer chute marked as (1), (2) and (3), respectively. A 3D model representation of the giant concrete batching plant is created and faceted using ANSYS Spaceclaim module. The STL files of the batching plant were created and mixer's rotational twin shaft speed (24 RPM) was set in LIGGGHTS UDF codes. Here, the mega bunker is designed such that the walls are steep enough decreasing friction effect relative to gravity in order to allow the aggregate and cement particles to slide down in a mass flow manner into the TSM. There is a 2500 litre capacity water tank in the left side of the Fig. 3(c), which is connected to the main body of the mixer via two water injection pipes.

In this study, we only consider the surface tension forces, but implementation of viscous forces will be carried out in the future works. The 6 m^3 TSM consists of two counter-rotating impellers with specifically designed robust blades. The blades have two folded profiles to minimize the wear and to allow longer durability.

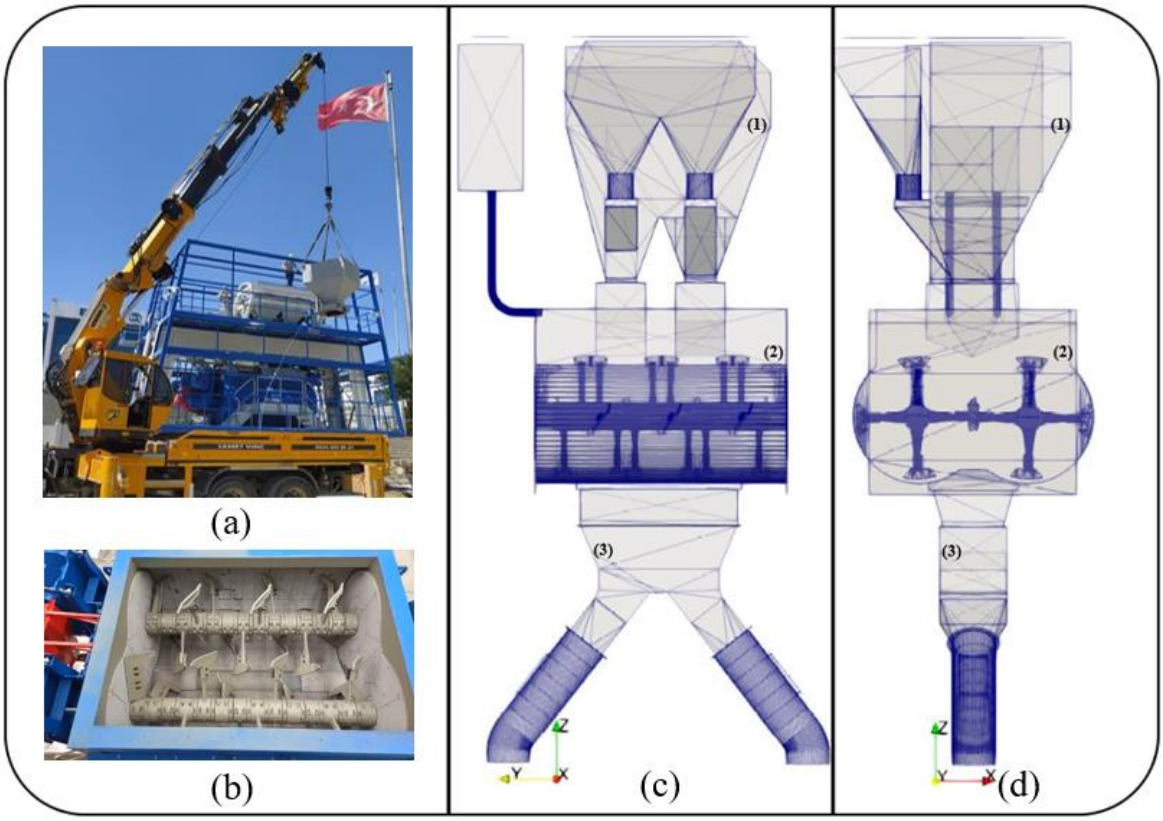

Figure 3. Assembly operation view (a), top view of mixer (b), front view (c) and side view (d) of 6 m^3 TSM fully equipped with mega bunker and controllable double side transfer chute

Two types of solid granular particles with different physical and mechanical characteristics are generated within the model. Mechanical and physical properties of particles were set to the average according to previous studies [30,38]. Properties of the aggregate, cement and structure in mega bunker and 6 m^3 TSM are given in Table 1 and Table 2, respectively.

Table 1: Properties of particles and walls in mega bunker used in the simulation

Material properties	**Particle 1(Aggregate)**	**Particle 2(Cement)**	**Wall**
Density(kg/m^3)	1400	800	7800
Radius (mm)	15	2.5	-

Young's Modulus (N/m^2)	50×10^6		50×10^6		210×10^9
Poisson Ratio	0.30		0.30		0.32
Contact Properties	**Particle 1-Particle 1**	**Particle 2-Particle 2**	**Particle 1-Particle 2**	**Particle 1-Wall**	**Particle2-Wall**
Sliding Friction Coefficient	0.52	0.40	0.46	0.50	0.30
Rolling Friction Coefficient	0.30	0.20	0.25	0.02	0.01
Coefficient of Restitution	0.60	0.60	0.60	0.60	0.60

Table 2: Properties of particles and walls in $6\ m^3$ *TSM used in the simulation*

Material Properties	**Particle 1(Mixture)**		**Particle 2(Mixture)**		**Wall**
Density(kg/m^3)	2400		2400		7800
Radius (mm)	15, 20		2.5, 20		-
Young's Modulus (N/m^2)	50×10^6		50×10^6		210×10^9
Poisson Ratio	0.30		0.30		0.32
Contact Properties	**Particle 1-Particle 1**	**Particle 2-Particle 2**	**Particle 1-Particle 2**	**Particle 1-Wall**	**Particle 2-Wall**
Sliding Friction Coefficient	0.52	0.40	0.46	0.50	0.30
Rolling Friction Coefficient	0.30	0.20	0.25	0.02	0.01
Coefficient of Restitution	0.10	0.10	0.10	0.10	0.10
Cohesion (J/m^3)	250000	250000	250000	250000	250000

According to the Rayleigh method given in Eq. (19), a minimum time step was calculated to guarantee accurate results. In each time step, the motions of all granular particles are computationally tracked, considering their interactions. The aforementioned forces and torques acting on particles are related to their motions. To make reliable simulation, a time step with millionth of a second is required to predict what happens in reality, which leads to greater computational cost [29]. Researchers recommended that the appropriate time step for simulating the dense particle motion was in the range of 20-80% of critical Rayleigh time step [39]. The simulation time step must be less than the critical Rayleigh time step TS_R.

$$TS < TS_R = \frac{\pi R}{(0.163v+0.8766)}\sqrt{\frac{\rho}{G}} \quad (19)$$

where, r, ρ, G and v are radius, density, shear modulus and poisson's ratio of particles respectively.

Open source Paraview software is used for the visualization of simulation. Paraview is multi-platform data analysis and visualization program. Also, Pizza compiler was used to prepare the output data of LIGGGHTS for Paraview.

3. Results

In the first simulation, four and half a million particles with two different sizes are generated randomly at spatial locations from two separate regions. These particles are deposited in the bunker under the effect of gravitational force. As shown in Fig. 4, the red and green particles represent aggregates and cement, respectively. The red and green particles are generated with aggregate and cement material properties given in Tables 1 and 2. The feeding process of 6 m^3 TSM is realized by two specially designed automatic hoppers. The bunker and mixer feeding simulations are realized by dry particles via Hertz-Mindlin's contact law and elastic-plastic spring-dashpot model. On the other hand, the mixing and discharging simulation of the mixer are accomplished by wet particles using the SJKR model. Fig. 4(b) and 4(c) illustrate aggregate and cement common ground area inside the bunker at simulation times 1.5 sec and 4 sec, respectively. In addition, a combination of segregation by percolation and momentum segregation has been demonstrated in Fig. 4(b) and 4(c).

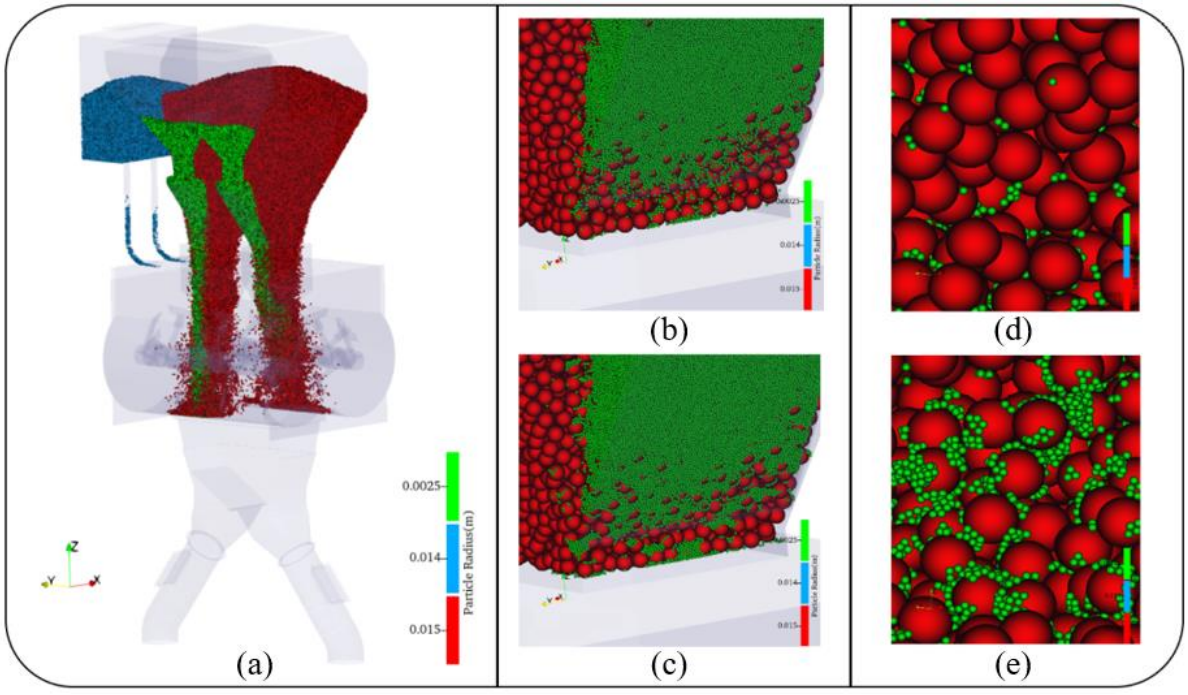

Figure 4. Simulation snapshots at different simulation times from isometric view of concrete plant (a), bunker area (b)-(c) and the inside of the mixer (d)-(e)

As time increases, the number of cement particles increases in the bottom part of the bunker due to the percolation effect. Segregation by percolation occurs owing to the small geometry of cement particles in comparison to that of aggregates. It is also observed that seeded granulation occurs during the wet mixing process. This seeding mechanism arises when aggregate particles become slightly wetted, act as a nucleus at the granules core, and finally get covered by cement particles [38]. Fig. 4(d) and 4(e) demonstrate mixtures seeded granulation at simulation times 15 sec and 25 sec, respectively. Eventually, the number of cement particles around aggregate particles rises dramatically as a result of cohesive force between particles.

Due to very long computational time, the simulation of the entire system with four and a half million particles couldn't be realized. Therefore, the second simulation with a smaller number of particles has been carried to analyze the mixing performance of the 6 m^3 TSM and transfer chute.

In the second simulation, 150,000 monosized particles designated with two different colors are generated and injected into the mixer. The total simulation time is 117 sec comprised of the filling, mixing, and discharging times of 12 sec, 64 sec, and 41 sec, respectively. Fig. 5 shows a series of snapshots from the TSM in different mixing times.

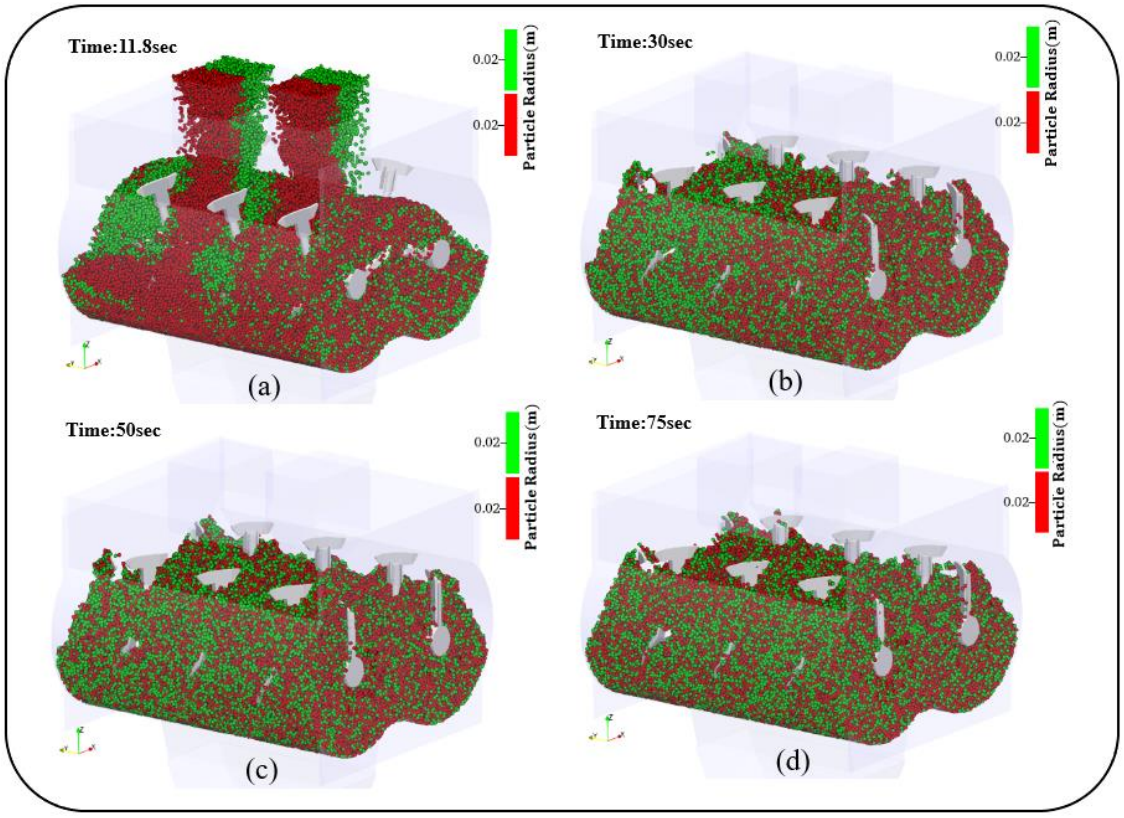

Figure 5. Simulation snapshots at different simulation times from isometric view of twin shaft mixer

Initially, the particles are partially mixed without cohesion effect during the filling time. Subsequently, the mixing process continues with the SJKR cohesion model. Theoretically, convection, diffusion and shearing are the most important mechanisms during the mixing process. For the fast mixing of particles at bulk scale, the convective mixing has the leading role, whereas diffusive mixing involves particle motions on the particle-length scale on newly developed surface regions [40]. As shown in Fig. 5(a), the convective and diffusive mixing is prevailing in the filling stage of the mixer. In addition, after the particle filling stage, the shear mixing is prevalent when the granular particles are mixed with cohesion effect. On the other hand, trajectory and percolation segregations have been perceived in the first stage of mixing in Fig. 5(a). Fig. 5(b), (c) and (d) demonstrate simulation snapshots from TSM at different times, 30 sec, 50 sec and 75 sec, respectively. After 64th sec of continuous mixing, the green particles are uniformly mixed within the whole TSM, indicating that the system has reached an overall homogeneous mixing state. In order to study the mixing performance of TSM, it is crucial to quantify the mixing index. Thus, we use statistical lacey and miles methods to quantize the mixing index [41].

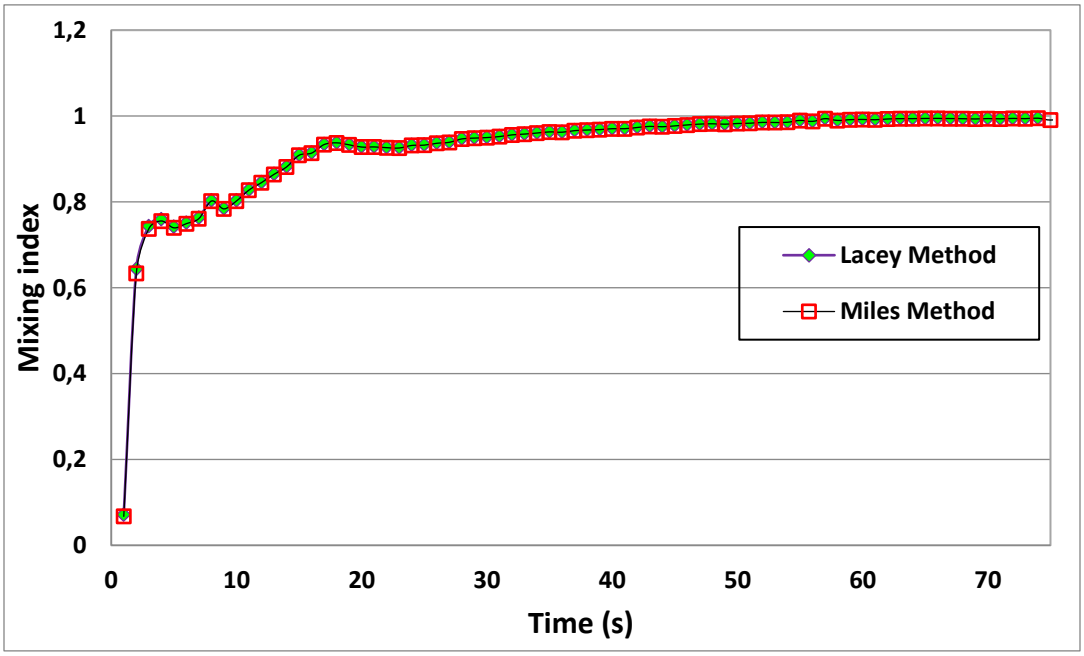

Figure 6. The mixing index versus time via two different statistical methods in the second simulation

The fewer mixture samples are studied, the more unreliable evaluation of the mixing index will be. Therefore, recommended mixture samples should be around 20-40 [41]. In this study, twenty-one mixture samples are extracted from different locations of the TSM at each second of the simulation time. Then, the mixing index for each second is computed by the lacey and miles methods, and the results are shown in Fig. 6. In addition,

the mixing index reaches a steady state after approximately thirty seconds. After forty seconds of mixing, the miles mixing index reaches one and arrives at a plateau, indicating the highest quality mixing performance. The good agreement between miles and lacey mixing index results indicates that the calculated values are accurate enough to rely on the simulation. On the other hand, the velocity distributions of particle regimes were compared qualitatively and quantitatively, and the results are shown in Fig. 7.

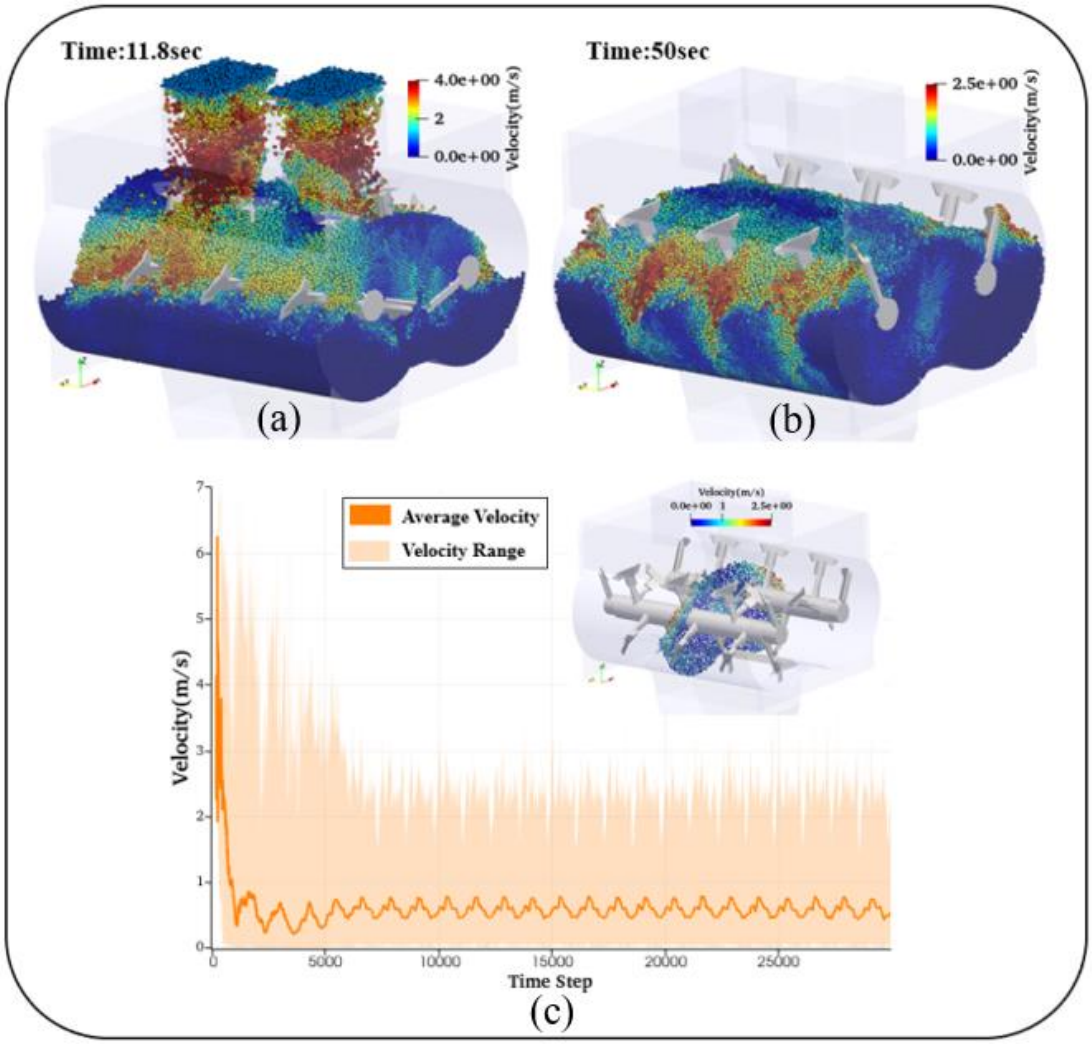

Figure 7. Simulation snapshots from velocity of particles in the 6 m^3 TSM (a)-(b) and the average particle velocity as a function of time step for extracted samples (c)

Fig. 7(a) and 7(b) represent velocity fields in the filling and mixing stages of the TSM, respectively. The particle flow regime comprises of active and passive layers. So, the particles can alter their position from the almost stagnant passive layer to the active layer and vice versa. This transition of particles occurs due to the combination of convection,

diffusion and shearing mechanism. The highest velocity fields are observed near the blades' motion directions which is known as active layers. On the other hand, the less active region with dark blue colors is known as passive layers in Fig. 7(b). In addition, the velocity field in Fig. 7(b) is scaled to the blade tip speed in order to realize the active and passive layers clearly. The kinetic energy of particles reaches its maximum threshold in blade rotation regions with a maximum velocity of ~2.5 m/s. It can be observed from Fig. 7(c) that the average velocity of particles oscillates between 0.54 m/s to 0.66 m/s when the filling stage of TSM is completed. To study the discharging performance of the double-side transfer chute, simulation snapshots from mixture flow patterns and the mixture throughput versus time are illustrated in Fig. 8.

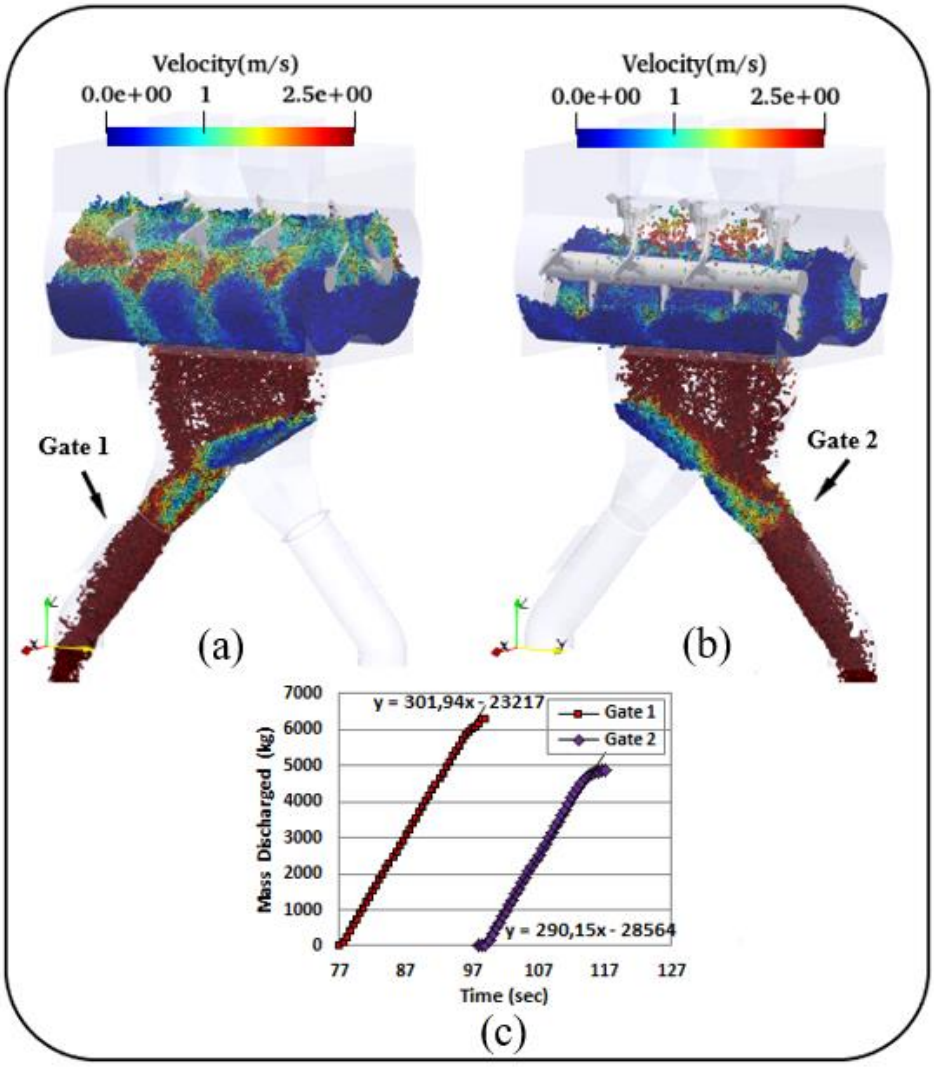

Figure 8. Particles flow pattern from TSM through double side transfer chute (a)-(b) and the mixture throughput with respect to time during discharging stage (c)

After the mixing stage is over, the bottom gate of the TSM is opened and the mixture moves into the desired gate under the effect of gravitational force. The diversion of the mixture from gate one towards gate two is realized via a hydraulically operating apron system. In Fig. 8(c), the first steep increase from zero to 6300 kg represents discharged mass through gate one in almost 22 sec. Also, the second steep increase from zero to 4870 kg demonstrates discharged mass through gate two in 19 sec. In addition, the slope of the first and the second steep increase represents throughput values of 301 kg/s and 290 kg/s for gate one and gate two, respectively.

4. Discussion and Conclusion

Numerical simulations using the discrete element method (DEM), which is a robust technique for studying granular flow, were utilized to simulate the filling, mixing and discharging performance of the concrete batching plant. For the sake of simulating dry particles in filling mega bunker and 6 m3 twin shaft mixer, Hertz-Mindlin's contact law and elastic-plastic spring-dashpot model were realized. Thereafter, simulation of wet particles in the mixer is accomplished via the SJKR model. Also, the segregation by percolation and momentum segregation were observed during the bunker filling stage and the seeded granulation has occurred in the mixer for the first simulation when the radii of particles are not monosized. In addition, the second simulation was accomplished to study the full mixing period, which is an important factor for the quantification of the mixing index. After 30 seconds of mixing, the mixing index reaches the steady state and after 40 seconds of mixing, the mixing index reaches the highest value, which is fulfilling the expectation for the good quality of granular particles mixing. During the mixing stage, the maximum velocity fields were captured near the blades' rotation regions with a velocity of 2.5 m/s, magnitude. At last, mixture throughput from each gate was investigated, recognizing achieved values of 301 kg/s and 290 kg/s for gate one and two, respectively.

5. Acknowledge

The author would like to thank the Elkon Factories Chairman Mr. Mustafa Alpagut for funding this project. The author would also like to thank Prof. Dr. Kadir Kırkköprü for his invaluable advice. This research was supported by the Scientific and Technological Research Council of Turkey (TÜBİTAK) with the grant number 3189080.

References

[1] Paul, E. L., Atiemo-Obeng, V. A., & Kresta, S. M. (2004). *Handbook of Industrial Mixing*. John Wiley & Sons.

[2] Hassanpour, A., Tan, H., Bayly, A., Gopalkrishnan, P., Ng, B., & Ghadiri, M. (2011). Analysis of particle motion in a paddle mixer using Discrete Element Method (DEM). *Powder Technology*, *1–2*, 189–194. https://doi.org/10.1016/j.powtec.2010.07.025

[3] Xia, R., Wang, X., Li, B., Wei, X., & Yang, Z. (2019). Discrete Element Method- (DEM-) Based Study on the Wear Mechanism and Wear Regularity in Scraper Conveyor Chutes. *Mathematical Problems in Engineering*, 1–12. https://doi.org/10.1155/2019/4191570

[4] Schmelzle, S., & Nirschl, H. (2018). DEM simulations: mixing of dry and wet granular material with different contact angles. *Granular Matter*, *2*. https://doi.org/10.1007/s10035-018-0792-3

[5] Bertrand, F., Leclaire, L.-A., & Levecque, G. (2005). DEM-based models for the mixing of granular materials. *Chemical Engineering Science*, *8–9*, 2517–2531. https://doi.org/10.1016/j.ces.2004.11.048

[6] Abouzeid, A.-Z. M., & Fuerstenau, D. W. (2010). Mixing–demixing of particulate solids in rotating drums. *International Journal of Mineral Processing*, *1–4*, 40–46. https://doi.org/10.1016/j.minpro.2010.03.006

[7] Alian, M., Ein-Mozaffari, F., Upreti, S. R., & Wu, J. (2015). Using discrete element method to analyze the mixing of the solid particles in a slant cone mixer. *Chemical Engineering Research and Design*, 318–329. https://doi.org/10.1016/j.cherd.2014.07.003

[8] Lu, L.-S., & Hsiau, S.-S. (2008). Mixing in a vibrated granular bed: Diffusive and convective effects. *Powder Technology*, *1*, 31–43. https://doi.org/10.1016/j.powtec.2007.07.036

[9] Sinnott, M. D., & Cleary, P. W. (2015). The effect of particle shape on mixing in a high shear mixer. *Computational Particle Mechanics*, *4*, 477–504. https://doi.org/10.1007/s40571-015-0065-4

[10] Sato, Y., Nakamura, H., & Watano, S. (2008). Numerical analysis of agitation torque and particle motion in a high shear mixer. *Powder Technology*, *2*, 130–136. https://doi.org/10.1016/j.powtec.2007.11.028

[11] Hlosta, J., Jezerská, L., Rozbroj, J., Žurovec, D., Nečas, J., & Zegzulka, J. (2020). DEM Investigation of the Influence of Particulate Properties and Operating Conditions on the Mixing Process in Rotary Drums: Part 2—Process Validation and Experimental Study. *Processes*, *2*, 184. https://doi.org/10.3390/pr8020184

[12] Moakher, M., Shinbrot, T., & Muzzio, F. J. (2000). Experimentally validated computations of flow, mixing and segregation of non-cohesive grains in 3D tumbling blenders. *Powder Technology*, *1–3*, 58–71. https://doi.org/10.1016/s0032-5910(99)00227-2

[13] Washino, K., Chan, E. L., Miyazaki, K., Tsuji, T., & Tanaka, T. (2016). Time step criteria in DEM simulation of wet particles in viscosity dominant systems. *Powder Technology*, 100–107. https://doi.org/10.1016/j.powtec.2016.08.018

[14] Norouzi, H. R., Zarghami, R., Sotudeh-Gharebagh, R., & Mostoufi, N. (2016). *Coupled CFD-DEM Modeling*. John Wiley & Sons.

[15] TANG, P., & PURI, V. M. (2004). Methods for Minimizing Segregation: A Review. *Particulate Science and Technology*, *4*, 321–337. https://doi.org/10.1080/02726350490501420

[16] Kim, K.-M., Bae, J.-H., Park, J.-I., & Han, J.-W. (2019). Segregation Charging Behavior of Ultra-Fine Iron Ore Briquette in Sinter Feed Bed: DEM Analysis. *Metals and Materials International*, *8*, 1218–1225. https://doi.org/10.1007/s12540-019-00415-y

[17] Ma, X., Zhang, Y., Ran, H., & Zhang, Q. (2016). Segregation simulation of binary granular matter under horizontal pendulum vibrations. *International Journal of Modern Physics B*, *30*, 1650214. https://doi.org/10.1142/s0217979216502143

[18] Rhodes, M. J. (2013). *Introduction to Particle Technology*. John Wiley & Sons.

[19] LIGGGHTS, LAMMPS Improved for General Granular and Granular Heat Transfer Simulations Retrieved from http://www.cfdem.com

[20] LAMMPS, LAMMPS User Manual, Sandia National Laboratories, USA. (Retrieved from http://lammps.sandia.gov/doc/Manual.html).

[21] Mohanty, R., Mohanty, S., & Mishra, B. K. (2016). Study of flow through a packed bed using discrete element method and computational fluid dynamics. *Journal of the Taiwan Institute of Chemical Engineers*, 71–80. https://doi.org/10.1016/j.jtice.2016.03.025

[22] Komatsuzaki, T., & Iwata, Y. (2016). A combined approach for modeling particle behavior in granular impact damper using discrete element method and cellular automata. *International Journal of Mechanics and Materials in Design*, *3*, 407–417. https://doi.org/10.1007/s10999-016-9344-3

[23] Cleary, P. W., & Prakash, M. (2004). Discrete–element modelling and smoothed particle hydrodynamics: potential in the environmental sciences. *Philosophical Transactions of the Royal Society of London. Series A: Mathematical, Physical and Engineering Sciences*, *1822*, 2003–2030. https://doi.org/10.1098/rsta.2004.1428

[24] Cundall, P. A., & Strack, O. D. L. (1979). A discrete numerical model for granular assemblies. *Géotechnique*, *1*, 47–65. https://doi.org/10.1680/geot.1979.29.1.47

[25] Derakhshani, S. M., Schott, D. L., & Lodewijks, G. (2015). Micro–macro properties of quartz sand: Experimental investigation and DEM simulation. *Powder Technology*, 127–138. https://doi.org/10.1016/j.powtec.2014.08.072

[26] Smith, W., & Peng, H. (2013). Modeling of wheel–soil interaction over rough terrain using the discrete element method. *Journal of Terramechanics*, *5–6*, 277–287. https://doi.org/10.1016/j.jterra.2013.09.002

[27] Iwashita, K., & Oda, M. (1998). Rolling Resistance at Contacts in Simulation of Shear Band Development by DEM. *Journal of Engineering Mechanics*, *3*, 285–292. https://doi.org/10.1061/(asce)0733-9399(1998)124:3(285)

[28] Malone, K. F., & Xu, B. H. (2008). Determination of contact parameters for discrete element method simulations of granular systems. *Particuology*, *6*, 521–528. https://doi.org/10.1016/j.partic.2008.07.012

[29] Li, T., Peng, Y., Zhu, Z., Zou, S., & Yin, Z. (2017a). Discrete Element Method Simulations of the Inter-Particle Contact Parameters for the Mono-Sized Iron Ore Particles. *Materials*, *5*, 520. https://doi.org/10.3390/ma10050520

[30] Kenneth Langstreth, J., Kendall, K., & A.D., R. (1971). Surface energy and the contact of elastic solids. *Proceedings of the Royal Society of London. A. Mathematical and Physical Sciences*, *1558*, 301–313. https://doi.org/10.1098/rspa.1971.0141

[31] Derjaguin, B. V., Muller, V. M., & Toporov, Yu. P. (1975). Effect of contact deformations on the adhesion of particles. *Journal of Colloid and Interface Science*, *2*, 314–326. https://doi.org/10.1016/0021-9797(75)90018-1

[32] Navarro, H. A., & de Souza Braun, M. P. (2013). Determination of the normal spring stiffness coefficient in the linear spring–dashpot contact model of discrete element method. *Powder Technology*, 707–722. https://doi.org/10.1016/j.powtec.2013.05.049

[33] Ucgul, M., Fielke, J. M., & Saunders, C. (2014). 3D DEM tillage simulation: Validation of a hysteretic spring (plastic) contact model for a sweep tool operating in a cohesionless soil. *Soil and Tillage Research*, 220–227. https://doi.org/10.1016/j.still.2013.10.003

[34] Thornton, C. (1997). Coefficient of Restitution for Collinear Collisions of Elastic-Perfectly Plastic Spheres. *Journal of Applied Mechanics*, *2*, 383–386. https://doi.org/10.1115/1.2787319

[35] Hertz, H. (1882). Ueber die Berührung fester elastischer Körper. *Crll*, *92*, 156–171. https://doi.org/10.1515/crll.1882.92.156

[36] Chand, R., Khaskheli, M. A., Qadir, A., Ge, B., & Shi, Q. (2012). Discrete particle simulation of radial segregation in horizontally rotating drum: Effects of drum-length and non-rotating end-plates. *Physica A: Statistical Mechanics and Its Applications*, *20*, 4590–4596. https://doi.org/10.1016/j.physa.2012.05.019

[37] Walton, O. R. (n.d.). Potential Discrete Element Simulation Applications Ranging from Airborne Fines to Pellet Beds. *SAE Transactions*, *113*, 471–483. https://doi.org/10.2307/44737907

[38] Behjani, M. A., Rahmanian, N., Fardina bt Abdul Ghani, N., & Hassanpour, A. (2017). An investigation on process of seeded granulation in a continuous drum granulator using DEM. *Advanced Powder Technology*, *10*, 2456–2464. https://doi.org/10.1016/j.apt.2017.02.011

[39] O'Sullivan, C., & Bray, J. D. (2004). Selecting a suitable time step for discrete element simulations that use the central difference time integration scheme. *Engineering Computations*, *2/3/4*, 278–303. https://doi.org/10.1108/02644400410519794

[40] Cullen, P. J., Romañach, R. J., Abatzoglou, N., & Rielly, C. D. (2015). *Pharmaceutical Blending and Mixing*. John Wiley & Sons.

[41] Poux, M., Fayolle, P., Bertrand, J., Bridoux, D., & Bousquet, J. (1991). Powder mixing: Some practical rules applied to agitated systems. *Powder Technology*, *3*, 213–234. https://doi.org/10.1016/0032-5910(91)80047-m